Smart Structures and Systems, *Vol. 26, No. 2 (2020) 213-226*
DOI: https://doi.org/10.12989/sss.2020.26.2.213

Nonlinear buckling and free vibration of curved CNTs by doublet mechanics

Mohamed A. Eltaher*[1,2], Nazira Mohamed [3] and Salwa A. Mohamed [3]

[1] *Mechanical Engineering Department, Faculty of Engineering, King Abdulaziz University, P.O. Box 80204, Jeddah, Saudi Arabia*
[2] *Mechanical Design & Production Department, Faculty of Engineering, Zagazig University, P.O. Box 44519, Zagazig, Egypt*
[3] *Department of Engineering Mathematics, Faculty of Engineering, Zagazig University, P.O. Box 44519, Zagazig, Egypt*

(*Received November 17, 2019, Revised March 30, 2020, Accepted March 28, 2020*)

Abstract. In this manuscript, static and dynamic behaviors of geometrically imperfect carbon nanotubes (CNTs) subject to different types of end conditions are investigated. The Doublet Mechanics (DM) theory, which is length scale dependent theory, is used in the analysis. The Euler-Bernoulli kinematic and nonlinear mid-plane stretching effect are considered through analysis. The governing equation of imperfect CNTs is a sixth order nonlinear integro-partial-differential equation. The buckling problem is discretized via the differential-integral-quadrature method (DIQM) and then it is solved using Newton's method. The equation of linear vibration problem is discretized using DIQM and then solved as a linear eigenvalue problem to get natural frequencies and corresponding mode shapes. The DIQM results are compared with analytical ones available in the literature and excellent agreement is obtained. The numerical results are depicted to illustrate the influence of length scale parameter, imperfection amplitude and shear foundation constant on critical buckling load, post-buckling configuration and linear vibration behavior. The current model is effective in designing of NEMS, nano-sensor and nano-actuator manufactured by CNTs.

Keywords: imperfect CNTs; doublet mechanics theory; differential-integral-quadrature method (DIQM); buckling; vibration

1. Introduction

Recently, massive development of science and technology have a tendency to an era of nanotechnology. The progress in many fields, such as, material science, engineering, naval, aerospace, automotive, chemical, medicine, and electronics will enhance the easiness and leisurely of our life. Nanostructures such as, nanobars, nanotubes, nanobeams and nanoplates and nanogears are essential element utilized and exploited in nanotechnology. Since 1991, Iijima had discovered carbon nanotube (CNT), that has been considered by lots of researchers and scientists. Till now, CNT considers the strongest and most resilient material known, in addition to extraordinary mechanical, physical, and electrical properties, Eltaher *et al.* (2016a).

To understand and predict mechanical and physical behaviors of CNTs precisely, discrete or modified continuum models have to be included in the analysis and formulation rather than classical continuum theories, those are missing length-scale effect. In discrete models, such as, ab initio calculations and derivation (Hehre 1976, Kresse and Hafner 1993, and Peng and Cho 2003), quantum mechanics (QM) (Gao *et al.* 1998 and Atkins and Friedman 2011), molecular dynamic (MD) (Zhou and Shi 2002 and Rapaport and Rapaport 2004), simplifications, such as regularity of particle distribution, symmetry and periodicity are assumed. To consider a size dependency, modified continuum models such as nonlocal theories (Eringen 1972), modified couple stress theory of Mindlin (1963) and Toupin (1962), strain gradient theory (Yang *et al.* 2002), and surface energy (Gurtin and Murdoch 1975) were exploited.

Based on discreated models, Li and Chou (2003, 2004) investigated stability behaviors of CNTs under axial and bending loading conditions in frame of the molecular structural mechanics. In 2005, Xiao *et al.* established analytical molecular mechanics model to predict mechanical properties of defect-free CNTs by modified Morse potential function. Eltaher *et al.* (2016a) considered size-scale effect and material-dependency to illustrate the nonlinear static behavior of CNTs. Through molecular dynamics (MD) theory, Mehralian *et al.* (2017) explored the role of vacancy defects in thermal buckling of pre-compressed CNTs. By using the nonlocal temperature dependent, Shokravi and Jalili (2017) investigated dynamic buckling of sandwich micro plates reinforced by functionally graded CNTs. Eltaher *et al.* (2018) examined vibration behaviors of single/multi-CNTs by exploited continuum-discreated model including the energy equivalent between CNT atoms. Shokravi (2018) applied piezoelasticity theory to study dynamic buckling of the smart beam rested on Pasternak foundation and subjected to electric field. Akgöz and Civalek (2018) explored thermo-elastic vibrational behavior of thick microbeams rested in elastic foundation by modified couple stress theory. In frame of MD finite element method. Eltaher *et al.* (2019a)

*Corresponding author, Professor,
E-mail: meltaher@kau.edu.sa; mmeltaher@zu.edu.eg
[a] Professor
[b] Student

http://www.techno-press.org/?journal=sss&subpage=7
ISSN: 1738-1584 (Print), 1738-1991 (Online)

used energy equivalent model and finite element method to predict equivalent Young's modulus of SWCNT and its mechanical behaviors such as tension, buckling and vaibrations. Eltaher *et al*. (2019b, c) modified the previous model to consider defects and gaps included in CNTs and presented their modal participation factors. Eltaher *et al*. (2019d) and Mohamed *et al*. (2019) exploited MD and associated energy equivalent model to study post-buckling of curved CNTs in frame of nonlinear Euler-Bernoulli beam. Eltaher and Mohamed (2020a) presented a comprehensive model to investigate a free vibration and resonance frequencies of nanostructure perforated beam element as nano-resonator. Eltaher *et al*. (2020) developed a modified continuum model to explore and investigate static and vibration behaviors of perforated piezoelectric NEMS structure. Mohamed *et al*. (2020) studied post-buckling of CNTs by using higher order shear deformation and energy equivalent method. Based of classical MD, buckling behavior of covalently functionalized SWCNTs and DWCNTs was studied by Ameri *et al*. (2020).

In general, continuum theories are neglected size-dependent of micro/nano-level by identifying mechanical properties such as, Young's modulus, shear modulus, yield stress, and ultimate strength directly from macroscopic experiments, Ferrari *et al*. (1997). To overcome this deficiency and inconsistency, modified continuous mechanics models are proposed to take into account the missing information of micro/nano-level. Akgöz and Civalek (2011) studied via modified strain gradient elasticity theory buckling of protein microtubules. Eltaher *et al*. (2013) presented the coupling effect of nonlocal and surface energy on the vibration of nanobeam. Tounsi *et al*. (2013) examined the buckling stability of DWCNTs under a thermal load using nonlocal Timoshenko beam model. Eltaher *et al*. (2014a, b) exploited the higher order gradient theory to investigate the mechanical behaviors of nanbeams by finite element. Eltaher and Agwa (2016) and Agwa and Eltaher (2016) studied vibration behaviors of a pretension CNTs and carbyne nano-sensors by including surface elasticity, residual surface tension and nonlocal effect. Eltaher *et al*. (2016b) exploited Euler–Bernoulli nonlocal Eringen nanobeam to show long-range interactions between CNT atoms through vibration analysis. Ellali *et al*. (2018) studied buckling of piezoelectric plates rested on Pasternak elastic foundation using higher-order shear deformation plate theories. Tabbakh and Nasihatgozar (2018) studied buckling behavior of nanocomposite plates coated by magnetostrictive layer. Emam *et al*. (2018) examined post-buckling and vibration responses of imperfect multilayer nanobeams under compressive force. Mohamed *et al*. (2018) introduced a novel model to predict nonlinear forced vibrations of C-C curved beam in the locality of post-buckling mode. Youcef *et al*. (2018) developed an analytical non-classical model to predict the free vibrations of nanobeams included surface stress effects. Eltaher *et al*. (2019e) presented effects of periodic and nonperiodic modes on post-buckling and nonlinear vibration of beams rested on nonlinear foundations. Amir *et al*. (2019) studied vibration of FG saturated porous annular/circular micro sandwich plates embedded with CNTs subjected to multi-physical preloads. Arda and Aydogdu (2020) analyzed dynamic response of a carbon nanotube mass sensor by considering both inertia and stiffness of the detected mass. Arani *et al*. (2019) studied wave propagation of FG nano-beams based on the nonlocal elasticity theory considering surface and flexoelectric effects. Boussoula *et al*. (2020) presented a simple nth-order shear deformation theory for thermomechanical bending analysis of different configurations of FG sandwich plates. Civalek *et al*. (2020) studied size-dependent transverse and longitudinal vibrations of embedded carbon and silica carbide nanotubes by nonlocal finite element method.

To bridge the gap between discrete and continuous models, Doublet Mechanics (DM) has been proposed. This theory is introduced in 1993 by Granik and Ferrari, on the basis of linearly elasto-static geomechanical principles. Subsequently, it is broadened to encompass other domains, such as, elastodynamics, viscoelasticity, failure theories, homogenization, and thermomechanics, Ferrari *et al*. (1997). Doublet Mechanics is a discrete micro-model, in which solids are described by arrays of points and a specified distance between particles. A particle pair is known as a doublet, and the particle spacing introduces length scales into the micro-structural theory. The model acquires micro-stress and micro-strain constitutive laws between the particles in each doublet. The potential of doublet mechanics is considering the microstructural elongation strains with additional macrostrain elongation. *The theory has shown a promise to predict behaviors of nanotubes that are not presented by continuum mechanics*. Kojic *et al*. (2011) presented a FE formulation including a micro-strain by using DM to explain multiscale-multidomain modeling of microstructural materials. Eberhardt and Wallmersperger (2014) calculated the mechanical properties of SWCNTs numerically by using molecular mechanics approach, by considering the nanotube geometry and covalent bond. Fatahi-Vajari and Imam (2016a, b) derived a fourth-order partial differential equations governing the axial and torsional vibration modes of SWCNTs by using DM theory. Gul *et al*. (2017) and Gul and Aydogdu (2017) illustrated the axial vibration and flexural and axial wave propagation of CNTs embedded in an elastic medium using scale dependent DM theory. Gul and Aydogdu (2018a) investigated statics and dynamics of nanorods and nanobeams by using DM with implemented bond length of atoms of as an intrinsic length scale. The natural frequencies and critical buckling loads of perfect CNTs are investigated based on DM theory by Gul *et al*. (2018). In frame of DM, Gul and Aydogdu (2018b,2019) shown free vibration and buckling of DWCNTs embedded in an elastic medium with S-S boundary conditions. Yayli and Asa (2019) studied axial vibration of axially restrained CNTs within the framework of DM theory and Fourier sine series. Aydogdu and Gul (2018, 2020) studied buckling and vibration of double nanofibers embedded in an elastic matrix based on Euler-Bernoulli beam model. Based on DM theory, Eltaher and Mohamed (2020b) studied the static and dynamic behavior of perfect and imperfect CNTs. They developed closed form formulas for critical buckling loads and postbuckling configurations of perfect and imperfect

CNTs. As well as analytical solutions for linear vibration around buckled position were developed. C-C and S-S boundary conditions were considered.

To the author's knowledge, pre-buckling, post-buckling, and free vibration behaviors of perfect and imperfect SWCNTs with curved configuration in frame of DM theory and differential quadrature method have not been studied elsewhere. For this reason, this article intends to fill this gap in the literature and present comprehensive model to illustrate the mechanical behavior of size dependent SWCNTs in frame of DM. The rest of this manuscript is structured as follows: the main constitutive equations, micro-strain effects, geometrical imperfection of SWCNTs based on molecular dynamics are described in detail through section 2. The nonclassical sixth order nonlinear integro-partial differential equation of motion of imperfect SWCNT is derived through this section. Numerical solutions by using modified differential quadrature method of both perfect and imperfect CNTs are presented in section 3. Parametric studies are presented to discuss the effect of length scale parameter, imperfection amplitude and shear foundation constant on the buckling loads, static responses and natural frequencies of S-S and C-C CNTs are discussed in Section 4. Main observations, investigations and conclusions are briefed in Section 5. Appendix A presented the analytical solution for buckling and mode shape of clamped-simply supported CNTs.

2. Mathematical Model

2.1 Doublet mechanics constitutive

As known, a discreate doublet micro-mechanical model describes material's atoms by a set of array of points at predetermined distances. A pair of points is defined as a doublet, and spacing distances between points include length scales into the microstructural theory, as illustrated in Fig. 1. Any atom in array has translation and rotation motions, those can be expanded by Taylor series. The lowest order of expansion represents macro-strain, while the terms beyond the first produce micro-strain includes the multi length scale

Proposed that, the displacement field is concurring with displacement of an atom, thus, the elongation can be depicted by Ferrari *et al.* (1997)

$$\Delta u_\alpha = u(h+\zeta_\alpha^0, t) - u(h,t) \tag{1}$$

in which h is a position vector of an atom, ζ_α^0 is the separation distance, α is the doublets number, and t is the time. The micro-strain elongation is calculated by Ferrari *et al.* (1997)

$$\epsilon_\alpha = \frac{\tau_\alpha \,.\, \Delta u_\alpha}{\eta_\alpha} = \sum_{\chi=1}^{M} \frac{(\eta_\alpha)^{\chi-1}}{\chi!} \tau_\alpha^0 . (\tau_\alpha^0 . \nabla)^\chi \, u \tag{2}$$

in which τ_α is the unit vector through α direction, $\eta_\alpha = |\zeta_\alpha^0|$ is the doublet separation (interpoint) distance in the undeformed form, ∇ is the Del operator, and M is the number of terms in Taylor series expansion.

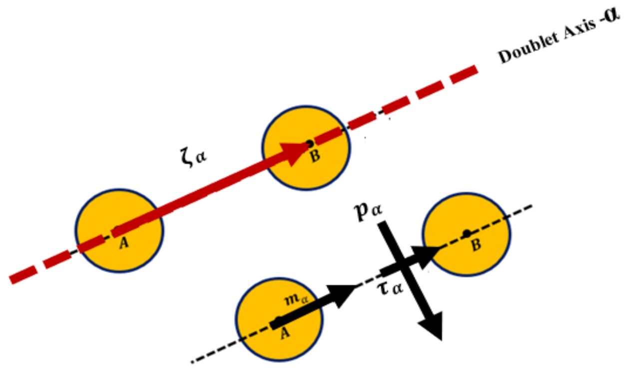

Fig. 1 Geometrical micro-strains of doublet mechanics

In linear elasticity, the relative displacement is small compared to doublet distance, so $\tau_\alpha = \tau_\alpha^0$. By considering the terms of Taylor series ($M = 3$), the micro-strains can be depicted in cartesian coordinate by Aydogdu and Gul (2018)

$$\epsilon_\alpha = \tau_{\alpha m}^0 \tau_{\alpha n}^0 \left(\varepsilon_{mn} + \frac{1}{2} \eta_\alpha \tau_{\alpha s}^0 \frac{\partial \varepsilon_{mn}}{\partial x_s} + \frac{1}{6} \eta_\alpha^2 \tau_{\alpha l}^0 \tau_{\alpha s}^0 \frac{\partial^2 \varepsilon_{mn}}{\partial x_l \partial x_s} \right) \tag{3}$$

If the number of expansion terms increased more than 3, the calculation will be more complicated. The micro-stress P_α can be described by

$$P_\alpha = \sum_\beta B_{\alpha\beta} \epsilon_\beta = B_0 \tau_{\alpha m}^0 \tau_{\alpha n}^0 \left(\varepsilon_{mn} + \frac{1}{2} \eta_\alpha \tau_{\alpha s}^0 \frac{\partial \varepsilon_{mn}}{\partial x_s} + \frac{1}{6} \eta_\alpha^2 \tau_{\alpha l}^0 \tau_{\alpha s}^0 \frac{\partial^2 \varepsilon_{mn}}{\partial x_l \partial x_s} \right) \tag{4}$$

where $B_{\alpha\beta}$ is the tension modulus between points α and β. The macro-stress can be written in terms of micro-stresses by

$$\sigma = \sum_{\alpha=1}^{n} \tau_\alpha^0 \, \tau_\alpha^0 \sum_{\chi=1}^{M} \frac{(-\eta_\alpha)^{\chi-1}}{\chi!} \tau_\alpha^0 . (\tau_\alpha^0 . \nabla)^{\chi-1} \; P_\alpha \tag{5}$$

Substituting Eq. (4) into Eq. (5), results the macro-stress in terms of macro/micro-strains as

$$\sigma = \sum_{\alpha=1}^{n} B_0 \tau_{\alpha i}^0 \tau_{\alpha j}^0 \tau_{\alpha m}^0 \tau_{\alpha n}^0 \left(\varepsilon_{mn} + \frac{1}{12} \eta_\alpha^2 \tau_{\alpha l}^0 \tau_{\alpha s}^0 \frac{\partial^2 \varepsilon_{mn}}{\partial x_l \, \partial x_s} \right) \tag{6}$$

Since beam and plate theories are based on plane stress relations, thus $-\frac{\varepsilon_{33}}{\varepsilon_{11}} = -\,-\frac{\varepsilon_{22}}{\varepsilon_{11}} = \nu = \frac{1}{3}$. According to Euler-Bernoulli beam theory, the normal stress including the DM micro-strain can be described as

$$\sigma_{xx} = B_0\left(\varepsilon_{xx} + \frac{1}{12}\eta_\alpha^2\frac{\partial^2\varepsilon_{xx}}{\partial x^2}\right) = \varkappa_0\sigma_{xx}^{LE} + \varkappa_1\sigma_{xx}^{DM} \quad (7)$$

where $\varkappa_0 = 1$, $\varkappa_1 = \frac{1}{12}\eta_\alpha^2$, σ_{xx}^{LE} is classical elastic stress and σ_{xx}^{DM} is the doublet stress due to micro-strain. The two parameters $\varkappa_0$ and $\varkappa_1$ are depending on the chirality angle of nanotube, angles between nodes, and number of terms of Taylor expansion. Plane stress condition leads to $B_0 = E$, where E is the Young's modulus, Gul *et al.* (2018).

2.2 Nanotube beam formulation

According to Euler-Bernoulli theory, the axial and lateral displacements, (U, W), of any common point located at $(x, 0, z)$ in the undeformed state of CNT are

$$\begin{aligned} &U(x,z,t) = u(x,t) - z\left[\frac{\partial W}{\partial x} - \frac{dw_0}{dx}\right] \\ &\& \quad W(x,z,t) = w(x,t) \end{aligned} \quad (8)$$

where u and w are the axial and transverse displacements, respectively, along centroidal axis of nanotube. w_0 is the initial rise (imperfection) of CNT beam structure. Thus, nonlinear axial strain including von Karman strain and micro-strain is governed by

$$\varepsilon_{eqx} = \varepsilon_{xx} + \frac{1}{12}\eta_\alpha^2\frac{\partial^2\varepsilon_{xx}}{\partial x^2} + \varepsilon_{mps} \quad (9)$$

where ε_{mps} is the nonlinear midplane stretching due to initial curvature and out of deformation, which can be evaluated by $\varepsilon_{mps} = \frac{1}{2}\left[\left(\frac{\partial W}{\partial x}\right)^2 - \left(\frac{dw_0}{dx}\right)^2\right]$. So, the force and moment resultants including micro-strain and mid-plane stretching and initial imperfection can be described by

$$\begin{aligned} &N = \int_A \sigma_{xx}dA = \int_A E\varepsilon_{eqx}dA \\ &\& \quad M = \int_A zE\varepsilon_{eqx}dA \end{aligned} \quad (10)$$

Equations of motion of imperfect DM carbon nanotube can be presented by

$$m\frac{\partial^2 u}{\partial t^2} + \mu_0\frac{\partial u}{\partial t} - \frac{\partial N}{\partial x} = F_u \quad (11a)$$

$$m\frac{\partial^2 w}{\partial t^2} + \mu_1\frac{\partial w}{\partial t} - \frac{\partial^2 M}{\partial x^2} - N\frac{\partial^2 w}{\partial x^2} = F_w + F_\Omega \quad (11b)$$

where the inertia term is $m = \int_A \rho dA$, F_u is the axial force along the x-axis, μ_0 and μ_1 are damping coefficients through axial and transverse directions, respectively. $F_\Omega = \bar{F}cos(\bar{\Omega}t)$ is the affected harmonic force and $F_w = \bar{k}_s\frac{\partial^2 w}{\partial x^2}$ is the transverse shear force. By substituting Eqs. (8) and (9) into Eq. (10), and then substitute results into Eq. (11), the following governing equation of motion of imperfect CNTs including mid-plane stretching and micro-strain is

$$\begin{aligned} &m\frac{\partial^2 w}{\partial t^2} + \bar{\mu}\frac{\partial w}{\partial t} + \frac{EI}{1-\nu^2}\left[\frac{\eta^2}{12}\left(\frac{\partial^6 w}{\partial x^6} - \frac{\partial^6 w_0}{\partial x^6}\right)\right. \\ &\left. + \left(\frac{\partial^4 w}{\partial x^4} - \frac{d^4 w_0}{dx^4}\right)\right] + \bar{P} - \bar{k}_s + \frac{AE}{2L(1-\nu^2)} \\ &\left.\int_0^L\left(\left(\frac{\partial w}{\partial x}\right)^2 - \left(\frac{dw_0}{dx}\right)^2\right)dx\right]\frac{\partial^2 w}{\partial x^2} = \bar{F}cos(\bar{\Omega}t) \end{aligned} \quad (12)$$

in which $\bar{\mu}$ is the damping coefficient, I is the moment of inertia, ν is the Poisson's ratio, A is the area of cross-sectional, L is the length of CNT, $\bar{P}$ is the applied axial load, $\bar{k}_s$ is the elastic shear stiffness parameter and $\eta = \eta_\alpha$ ($\eta = 0.1421\ nm$ for CNT). The boundary conditions (BCs) of the CNT can be described as

$$\text{C}-\text{C:} \quad w = \frac{\partial w}{\partial x} = \frac{\partial^3 w}{\partial \hat{x}} = 0 \quad at \quad x = 0, L \quad (13a)$$

$$\text{S}-\text{S:} \quad w = \frac{\partial^2 w}{\partial x^2} = \frac{\partial^2 w}{\partial x^2} + \frac{\eta^2}{12}\frac{\partial^4 w}{\partial x^4} = 0 \quad at \quad x = 0, L \quad (13b)$$

The generalized equation of motion of imperfect CNTs with DM micro-strains is described in nondimensional form as

$$\begin{aligned} &\ddot{w} + \mu\dot{w} + \beta^2\left(w^{vi} - w_0^{vi}\right) + \left(w^{iv} - w_0^{iv}\right) \\ &+ \left[P - k_s + \frac{1}{2}\int_0^1\left(w'^2 - w_0'^2\right)dx\right]w'' = Fcos(\Omega t) \end{aligned} \quad (14)$$

with the following nondimensional parameters

$$\begin{aligned} &\bar{x} = \frac{x}{L}, \quad \bar{w} = \frac{w}{r}, \quad \bar{w}_0 = \frac{w_0}{r}, \\ &r = \sqrt{\frac{I}{A}}, \quad \bar{t} = t\sqrt{\frac{EI}{(1-\nu^2)mL^4}} \end{aligned} \quad (15)$$

The coefficients of Eq. (14) are defined as

$$\begin{aligned} &\beta^2 = \frac{\eta^2}{12L^2}, \qquad P = \frac{\bar{P}L^2(1-\nu^2)}{EI}, \\ &k_s = \frac{\bar{k}_s L^2(1-\nu^2)}{EI}, \qquad \mu = \bar{\mu}\sqrt{\frac{L^4(1-\nu^2)}{mEI}}, \\ &F = \frac{L^4\bar{F}(1-\nu^2)}{EIr} \quad \text{and} \quad \Omega = \bar{\Omega}\sqrt{\frac{(1-\nu^2)mL^4}{EI}} \end{aligned} \quad (16)$$

Hence, nondimensional BCs are

$$w = w' = w''' = 0 \quad \text{at} \quad x = 0, 1 \quad \text{(Clamped BCs)} \quad (17a)$$

$$w = w'' = w'' + \beta^2 w^{iv} = 0 \quad \text{at} \quad x = 0, 1 \quad \text{(Simply supported BCs)} \quad (17b)$$

It should be noted that by setting $\beta = 0$ in Eq. (14), classical equation of motion is obtained. In Eq. (14), β

represents length scale of CNT.

3. Solution procedure

The solution of governing equation of imperfect CNTs, Eq. (14), can be split into two parts. A time-independent solution which is related to post-buckling analysis and time-dependent solution which is associated with dynamic analysis. Hence, the field variable of governing equation (14) is expressed as

$$w(x,t) = w_s(x) + w_d(x,t) \tag{18}$$

in which $w_s(x)$ is the static deflection due to applied axial load P and $w_d(x,t)$ is a small disturbance around the static deflection $w_s(x)$. Substituting Eq. (18) into the governing (14) and the equations of boundary conditions (17). Then collecting the static parts, the result is time-independent equation which represents the ***buckling problem*** of imperfect CNTs

$$\beta^2 w_s^{vi} + w_s^{iv} + \left[P - k_s - \frac{1}{2}\int_0^1 \left(w_s'^2 - w_0'^2\right)dx\right] w_s'' = \beta^2 w_0^{vi} + w_0^{iv} \tag{19}$$

The boundary conditions of Clamped and simply supported ends in static analysis are

$$C \qquad w_s = w_s' = w_s''' = 0 \quad \text{at} \quad x = 0, 1 \tag{20a}$$

$$S \qquad w_s = w_s'' = w_s'' + \beta^2 w_s^{iv} = 0 \quad \text{at} \quad x = 0, 1 \tag{20b}$$

Assembling the time-dependent parts around the static deflection position. The result is the following ***dynamic equation***

$$\begin{aligned}&\ddot{w}_d + \mu \dot{w}_d + \beta^2 w_d^{vi} + w_d^{iv} \\ &+ \left[P - k_s - \frac{1}{2}\int_0^1 \left(w_s'^2 - w_0'^2\right)dx\right] w_d'' - \frac{1}{2} w_s'' \int_0^1 w_d'^2 dx \\ &- w_s'' \int_0^1 w_d' w_s' dx - \frac{1}{2} w_d'' \int_0^1 w_d'^2 dx - w_d'' \int_0^1 w_d' w_s' dx \\ &= F cos(\Omega t)\end{aligned} \tag{21}$$

In terms of w_d, the boundary conditions are

$$C \qquad w_d = w_d' = w_d''' = 0 \quad \text{at} \quad x = 0, 1 \tag{22a}$$

$$S \qquad w_d = w_d'' = w_d'' + \beta^2 w_d^{iv} = 0 \quad \text{at} \quad x = 0, 1 \tag{22b}$$

Herein, the differential-integral-quadrature method is used as a numerical method to solve the governing equations of static and dynamic problems.

3.1 Differential-Integral-Quadrature Method (DIQM)

To discretize the domain, the shifted Chebyshev–Gauss–Lobatto grid points are used as, Mohamed *et al*. (2020)

$$x_i = \frac{1}{2}\left(1 - \cos\left(\frac{(i-1)\pi}{N-1}\right)\right), \quad i = 1,2,..N. \tag{23}$$

where N is the number of grid points in the whole computational domain. According to the DQM, the first-order derivative of a continuous function $y(x)$ is expressed as

$$\left.\frac{dy(x)}{dx}\right|_{x=x_i} = \sum_{j=1}^{N} \mathcal{C}_{ij}\, y(x_j), \quad i = 1,2,\cdots N \tag{24}$$

where $\mathcal{C}_{ij}$ is the weighting coefficients of the first order derivative which was introduced as

$$\mathcal{C}_{ij} = \begin{cases} \dfrac{\mathcal{P}(x_i)}{(x_i - x_j)\mathcal{P}(x_j)} & i \neq j \qquad i,j = 1,2,\ldots.N \\ -\displaystyle\sum_{j=1, i\neq j}^{N} \mathcal{C}_{ij} & i = j, \qquad i = 1,2,\ldots..N \end{cases} \tag{25}$$

in which

$$\mathcal{P}(x_i) = \prod_{j=1, j\neq i}^{N} (x_i - x_j) \tag{26}$$

Considering a vector $\boldsymbol{y} = [y(x_1)\, y(x_2) \ldots y(x_n)]^T$ and its first derivative vector to be $\boldsymbol{Y} = [Y(x_1)\, Y(x_2) \ldots Y(x_n)]$. Based on Eq. (26), a differential matrix of the first order derivative can be written as

$$\boldsymbol{Y} = C^{(1)}\, \boldsymbol{y} \tag{27}$$

where $C^{(1)} = [\mathcal{C}_{ij}]$. Using matrix multiplication, the higher order matrices can be obtained as

$$C^{(r)} = C^{(1)} C^{(r-1)}, r > 1 \tag{28}$$

The definite integral of a continuous function $y(x)$ over the domain can be obtained as

$$\frac{dy}{dx} = Y(x) \tag{29}$$

Then

$$\int_0^1 Y(x)dx \cong \sum_{k=1}^{N} ([\mathcal{K}]_{Nk} - [\mathcal{K}]_{1k}) Y_k = \boldsymbol{SF} \tag{30}$$

where $\mathcal{K}$ is the pseudo-inverse of matrix $C^{(1)}$. More explanations about DIQM are given is Mohamed *et al*. (2018).

3.2 Discritization of buckling problem of imperfect CNTs

The buckling problem (19) can be rewritten as

$$\beta^2 w_s^{vi} + w_s^{iv} + \gamma^2 w_s'' = \beta^2 w_0^{vi} + w_0^{iv} \tag{31a}$$

$$\gamma^2 = P - k_s - \frac{1}{2}\int_0^1 \left(w_s'^2 - w_0'^2\right)dx \tag{31b}$$

The column vector $\boldsymbol{w}_s$ can be defined as

$$\boldsymbol{w}_s^T = [w_1, w_2, \dots w_N] \tag{32}$$

in which $w_i = w(x_i)$. The initial shape of imperfection $w_0(x)$ is discretized as known vector $\boldsymbol{w}_0^T = [w_0(x_1), w_0(x_2), \dots, w_0(x_N)]$. Upon using the DIQM, the differential equation (34) can be discretized. The system of algebraic equations results from discretizing Eq. (34) is written as

$$\left(\beta^2 C^{(6)} + C^{(4)} + \gamma^2 C^{(2)}\right)\boldsymbol{w}_s - \left(\beta^2 C^{(6)} + C^{(4)}\right)\boldsymbol{w}_0 = \boldsymbol{0} \tag{33a}$$

$$\gamma^2 - P + k_s + \frac{1}{2}\boldsymbol{S}\left[\left(C^{(1)}\boldsymbol{w}_s\right)^{\circ 2} - \left(C^{(1)}\boldsymbol{w}_0\right)^{\circ 2}\right] = 0 \tag{33b}$$

where $\circ$ denotes matrix Hadamard product. The corresponding boundary conditions, Eq. (22), can be discretized in the same way and properly substituted in Eq. (33). To obtain buckling load and postbuckling configurations, the Newton method is used to solve nonlinear equations (33). The solution of the linearized form of Eq. (33) is considered as the initial values for Newton method.

3.3 Discritization of linear vibration problem

For linear vibration analysis, omitting the nonlinear, damping and force terms from Eq. (21), and using Eq. (31b), yields

$$\ddot{w}_d + \beta^2 w_d^{vi} + w_d^{iv} + \gamma^2 w_d'' - \frac{1}{2}w_s''\int_0^1 w_d'^2 dx = w_s''\int_0^1 w_d' w_s' dx \tag{34}$$

Assuming $w_d = \phi(x)e^{i\omega t}$ and inserting it in Eq. (34), on obtain

$$\beta^2\phi^{vi} + \phi^{iv} + \gamma^2\phi'' - \omega^2\phi = w_s''\int_0^1 w_s'\phi' dx \tag{35}$$

in which ω signifies the natural frequency and $\phi(x)$ is the corresponding mode shape. The boundary conditions are given as

$$C \quad \phi = \phi' = \phi''' = 0 \quad \text{at} \quad x = 0, 1 \tag{36a}$$

$$S \quad \phi = \phi'' = \phi'' + \beta^2\phi^{iv} = 0 \quad \text{at} \quad x = 0, 1 \tag{36b}$$

Using DIQM to discretize Eq. (35), the following linear eigenvalue problem is obtained

$$\left(\beta^2 C^{(6)} + C^{(4)} + \gamma^2 C^{(2)} - \left(\left[\left(C^{(2)}\boldsymbol{w}_s\right)\boldsymbol{O}^T\right] \circ \left[\boldsymbol{S}\left(C^{(1)}\boldsymbol{w}_s\right)C^{(1)}\right]\right)\right)\boldsymbol{\phi} = \omega^2\boldsymbol{\phi} \tag{37}$$

Similarly, the corresponding boundary conditions are discretized. where the unknown column vector $\boldsymbol{\phi}$ is defined as $\boldsymbol{\phi}^T = [\phi_1, \phi_2, \phi_3, \dots \dots \phi_N]$. The eigenvalue problem (37) can be easily evaluated for the eigenvalues ω and the corresponding mode shapes $\boldsymbol{\phi}$.

4. Numerical results

İn this section, numerical results for static and dynamic behaviors of perfect and imperfect CNTs are presented. The results based on DM and classical theories are compared and verified with those in the literatures. Herein, the initial shape of imperfection is assumed as the form of the first buckling mode shape of perfect CNT.

$$w_0 = \begin{cases} g\sin(\pi x) & \text{for S-S} \\ \frac{1}{2}g\left(1 - \cos(2\pi x)\right) & \text{for C-C} \end{cases} \tag{38}$$

Table 1 Comparison of the nondimensional first critical buckling load of S-S and C-C perfect CNTs when $k_s = 0$

L (nm)	S-S		C-C		
	DIQM	Gul (2018)	DIQM ($w''' = 0$)	DIQM ($w'' = 0$)	Gul (2018) ($w'' = 0$)
1	9.7057	9.711	36.8559	32.2056	32.21
1.5	9.7968	9.796	38.3129	34.3668	34.37
2	9.8287	9.828	38.8228	34.8952	34.89
5	9.8631	9.863	39.3736	38.1466	38.23
25	9.8694	-	39.4743	39.4806	-

Table 2 Nondimensional first three natural frequencies of S-S perfect CNTs ($k_s = 0, P = 0$)

Frequency mode		L (nm)					Classical
		1	1.5	2	5	20	
ω_1	DIQM	9.7873	9.8331	9.8491	9.8663	9.8694	9.8696
	Gul (2018)	9.787	9.833	9.849	9.849	-	9.869
ω_2	DIQM	38.1446	38.8913	39.1492	39.4259	39.4751	39.4784
	Gul (2018)	38.16	38.86	39.23	39.42	-	39.48
ω_3	DIQM	81.9195	85.8254	87.1510	88.5605	88.8098	88.8264
	Gul (2018)	81.92	85.82	87.15	88.56	-	88.83

For C-S CNT the shape of initial imperfection (shape of first buckling mode) can be obtained from Eq. (A8) in Appendix A.

4.1 Validation

To verify the accuracy of the present method, the dimensionless critical buckling load and the first three natural frequencies of perfect CNTs without applied load are compared with those available in literature. Table 1 compares the critical buckling load of S-S and C-C perfect CNTs based on the DIQM results and the results obtained by Gul *et al*. (2018). Since Gul *et al.* (2018) considered that the boundary conditions of C-C CNT take the form

$$w_s = w_s' = w_s'' = 0 \quad \text{at} \quad x = 0, 1 \tag{39}$$

In this table, the present model for C-C CNT is solved assuming the same form of boundary conditions. It can be found that the DIQM results are very close to those in the

Table 3 Comparison of the nondimensional first three critical buckling load of S-S, C-S and C-C perfect CNTs

B. Cs	k_s	$L(nm)$	Pc_1		Pc_2		Pc_3	
			DIQM	Analytical	DIQM	Analytical	DIQM	Analytical
S-S	0	1	9.7057	9.7057	36.8559	36.8558	75.5497	75.5496
		1.5	9.7968	9.7968	38.3129	38.3129	82.9257	82.9256
		2	9.8287	9.8286	38.8228	38.8227	85.5073	85.5072
		5	9.8631	9.8630	39.3735	39.3735	88.2954	88.2953
		25	9.8694	9.8693	39.4743	39.4742	88.8052	88.8052
		Classical	9.8697	9.8696	39.4785	39.4784	88.8265	88.8264
	5	1	14.7057	14.7057	41.8559	41.8558	80.5497	80.5496
		1.5	14.7968	14.7968	43.3129	43.3129	87.9257	87.9256
		2	14.8287	14.8286	43.8228	43.8227	90.5073	90.5072
		5	14.8631	14.8630	44.3735	44.3735	93.2954	93.2953
		25	14.8694	14.8693	44.4743	44.4742	93.8052	93.8052
		Classical	14.8697	14.8696	44.4785	44.4784	93.8265	93.8264
C-S	0	1	19.4302	19.4302	53.5072	53.5072	94.7106	94.7105
		1.5	19.8506	19.8505	56.9333	56.9332	108.1518	108.1517
		2	20.0046	20.0047	58.1328	58.1328	112.8538	112.8537
		5	20.1620	20.1605	59.4154	59.4316	117.9446	117.9320
		25	20.1897	20.1896	59.6698	59.6696	118.8617	118.8612
		Classical	20.1908	20.1907	59.6796	59.6795	118.8999	118.8998
	5	1	24.4302	24.4302	58.5072	58.5072	99.7106	99.7105
		1.5	24.8506	24.8505	61.9333	61.9332	113.1518	113.1517
		2	25.0046	25.0047	63.1328	63.1328	117.8538	117.8537
		5	25.162	25.1605	64.4154	64.4316	122.9446	122.932
		25	25.1897	25.1896	64.6698	64.6696	123.8617	123.8612
		Classical	25.1908	25.1907	64.6796	64.6795	123.8999	123.8998
C-C	0	1	36.8559	36.8559	68.429	68.429	115.9527	115.9526
		1.5	38.3129	38.3128	75.3477	75.346	139.2644	139.2643
		2	38.8228	38.8228	77.7209	77.7208	147.4235	147.4233
		5	39.3736	39.3735	80.3089	80.2818	156.2353	156.2353
		25	39.4743	39.4742	80.7449	80.7437	157.8466	157.8466
		Classical	39.4785	39.4784	80.763	80.7626	157.9137	157.9137
	5	1	41.8559	41.8559	73.429	73.429	120.9527	120.9526
		1.5	43.3129	43.3128	80.3477	80.346	144.2644	144.2643
		2	43.8228	43.8228	82.7209	82.7208	152.4235	152.4233
		5	44.3736	44.3735	85.3089	85.2818	161.2353	161.2353
		25	44.4743	44.4742	85.7449	85.7437	162.8466	162.8466
		Classical	44.4785	44.4784	85.763	85.7626	162.9137	162.9137

literature.

The dimensionless natural frequencies of S-S perfect CNTs obtained via DIQM and those reported by Gul *et al.* (2018) are compared in Table 2. Again, the results are found to be in good agreement.

4.2 Parametric studies

In this subsection, parametric studies are presented to analyze the influence of length-scale parameter, shear foundation constants and imperfection amplitude on the on buckling, post-buckling behavior and natural frequencies of CNTs.

4.2.1 Parametric studies of static analysis

The mutual effects of length scale and shear foundation constants on the dimensionless first three critical buckling loads of S-S, C-S and C-C perfect CNTs are summarized in Table 3. The DIQM results and analytical results reported by Eltaher and Mohamed (2020b) are presented. Based on Eltaher and Mohamed (2020b), the analytical solution for C-S perfect CNT is developed and is presented in Appendix A. It is found that increases the CNTs length increases the critical buckling loads. Also, it is observed that the critical buckling loads predicted by DM model are lower than those of the classical ones especially for higher buckling modes and short CNTs. Comparing the effect of length on different boundary conditions shows that the length-scale parameter is more effective in the case of C-C CNT. Furthermore, it should be pointed out that the critical buckling load are significantly increased with increasing the shear foundation constant.

The post-buckling paths of S-S, C-S and C-C perfect CNTs for diverse length values are demonstrated in Fig. 2. It can be seen that the maximum static deflection of CNT decreases significantly as the length of CNT increases. This means that the impact of length scale parameter cannot be ignored.

Table 4 summarizes the dimensionless first critical buckling loads of imperfect CNTs for diverse imperfection amplitude and length values with $k_s = 0$. Different set of boundary conditions are considered. It is noticed that as the length scale parameter increases (the length of CNTs decreases) causes the CNTs to behave softer and the critical buckling loads decrease. This softening behavior becomes more pronounced when the value of imperfection amplitude increases.

Fig. 3 depicts the variations of the dimensionless critical buckling load with the imperfection amplitude g for different values of CNTs length. Fig. 3 reveals that the

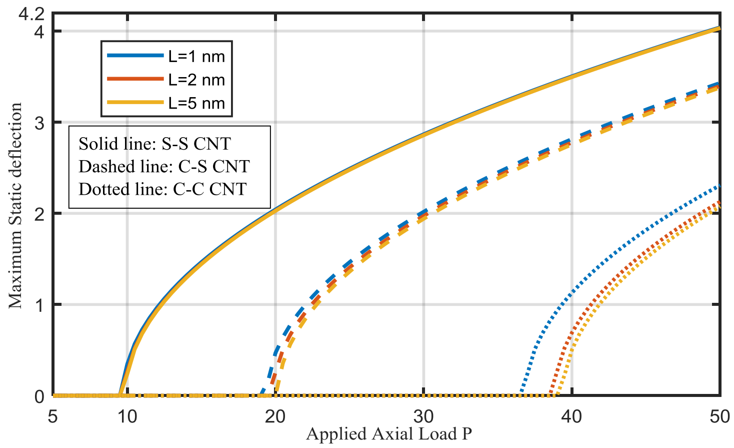

Fig. 2 Load-deflection curve of perfect S-S, C-S and C-C CNTs showing the lowest t buckled configurations when $k_s = 0$

Table 4 Nondimensional first critical buckling load of S-S, C-S and C-C imperfect CNTs when $k_s = 0$ and with various values of imperfection amplitude

B. Cs	g	L (nm)					Classical
		1	1.5	2	5	20	
S-S	0.5	16.4089	16.5457	16.5935	16.6452	16.6544	16.6550
	1	18.8582	19.0218	19.079	19.1408	19.1518	19.1525
	2	18.2815	18.4877	18.5598	18.6376	18.6515	18.6524
C-S	0.5	30.5825	31.1621	31.5131	31.6158	31.6538	31.6935
	1	35.5793	36.2571	36.6664	36.7864	36.8307	36.8756
	2	38.8488	39.6975	40.1753	40.322	40.3762	40.3777
C-C	0.5	54.056	55.9794	56.6513	57.3760	57.5054	57.5140
	1	62.6711	64.8686	65.6355	66.4625	66.6100	66.6198
	2	71.8821	74.5146	75.4324	76.4217	76.5982	76.6099

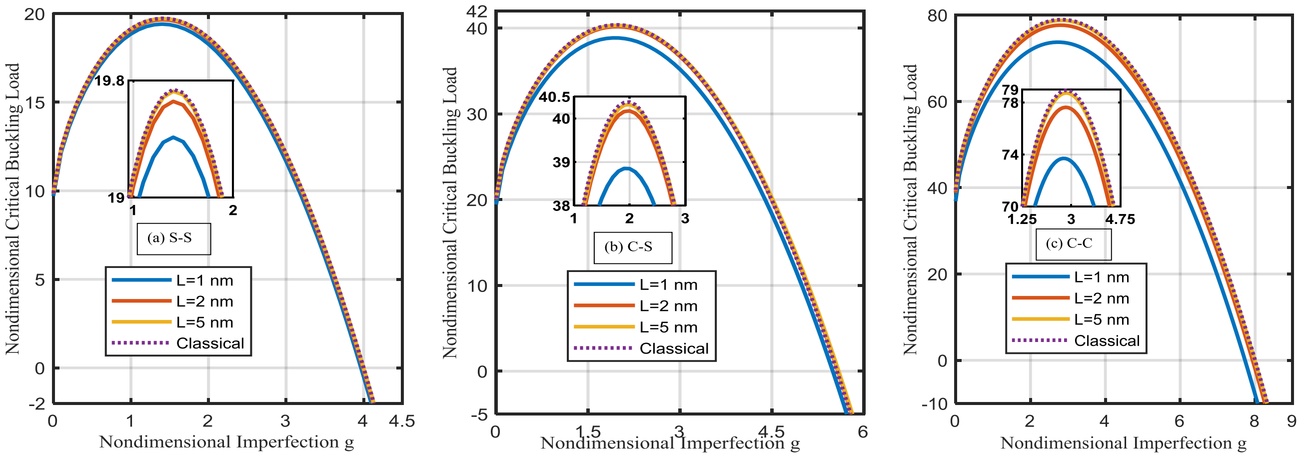

Fig. 3 Variation of the critical buckling load with the imperfection amplitude for different values of length L when $k_s = 0$

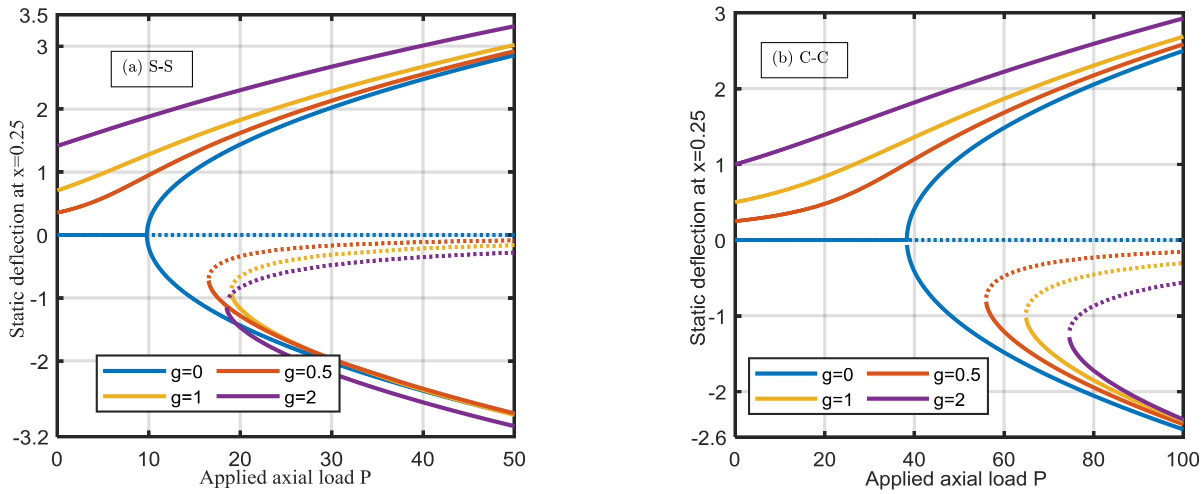

Fig. 4 Influence of dimensionless imperfection amplitude g on load-deflection curve of S-S and C-C CNTs ($k_s = 0,\ L = 1.5\ nm$)

critical buckling loads of imperfect CNTs with respect to g has a general tendency of ascending followed by descending for both DM and classical theories. It can be noted that as the effect of length scale parameter increases (CNTs length decrease), the difference between critical buckling loads predicted based on DM model and that obtained based on classical one increases, especially for C-C CNTs.

Fig. 4 shows the stable and unstable equilibrium paths of S-S and C-C perfect and imperfect CNTs for diverse values of imperfection amplitude when $L = 2\ nm$ and $k_s = 0$. The solid lines are associated with the stable responses and the dotted lines are associated with the unstable responses. It can be noted that perfect CNTs undergoes a pitchfork bifurcation. However, the imperfect CNTs exhibit a perturbed pitchfork (saddle-node) bifurcation. Fig. 4 illustrates that the imperfect CNTs in pre-buckling state ($P < P_c$), has a stable solution (upper branch) which is independent on the bifurcation phenomena. In the post-buckling state ($P > P_c$), middel unstable branch and lower stable one appear. Furthermore, it is observed that the absolute values of the amplitude of upper stable and the middle unstable responses increase as the imperfection amplitude increases.

In Fig. 5, the nonlinear responses of S-S and C-C imperfect CNTs in pre-and post-buckling states for different values of CNTs length are plotted. It is noticed that the absolute values of the amplitude of upper and lower stable branches decreases as the CNTs length increases. The reverse scenario occurs for the middle unstable branch.

4.2.2 Parametric studies of linear vibration

The first three dimensionless natural frequencies of S-S imperfect CNT at no axial load for diverse values of CNTs length and shear foundation constant are presented in Table 5. It is noticed the natural frequencies has an ascending trend with respect to shear foundation constant. That is due to the fact that the shear foundation constant increases the stiffness of CNTs. As consequence, the natural frequencies of CNTs increase with increasing the shear foundation parameter. Furthermore, it is observed that increasing the length of CNT, the results of DM model converge to classical results and length scale parameter becomes in significant. The effects of length scale parameter and shear

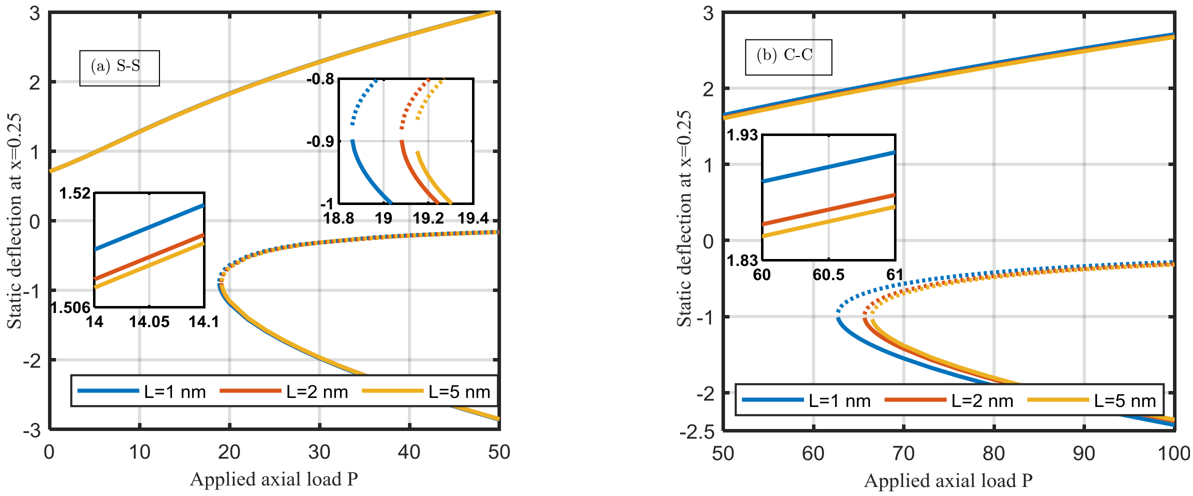

Fig. 5 Influence of length L on the load-deflection curves of S-S and C-C imperfect CNTs ($k_s = 0,\ g = 1$)

Table 5 Nondimensional first three natural frequencies of S-S imperfect CNTs with various values of shear foundation constant k_s, ($g = 1, P = 0$)

Frequency mode	k_s	L (nm) 1	1.5	2	5	20	Classical
ω_1	0	12.0206	12.0580	12.0710	12.0851	12.0876	12.0877
	5	12.5891	12.6313	12.6460	12.6619	12.6648	12.6650
	10	13.8374	13.8761	13.8894	13.9039	13.9065	13.9067
ω_2	0	38.1446	38.8913	39.1492	39.4259	39.4751	39.4784
	5	40.0656	40.7803	41.0269	41.2920	41.3392	41.3423
	10	42.2000	42.8807	43.1137	43.3661	43.4110	43.4140
ω_3	0	81.9195	85.8254	87.1510	88.5605	88.8098	88.8264
	5	83.9575	87.7755	89.0732	90.4537	90.6980	90.7143
	10	86.2781	89.9978	91.2639	92.6118	92.8505	92.8663

foundation constant are more pronounced in the higher modes.

Fig. 6 analyzes the variation of the dimensionless first natural frequency of S-S and C-C perfect CNTs under different values of CNTs length. In the pre-buckling state, increasing the CNTs length leads to increasing the natural frequency. However, in the postbuckling state, the reverse scenario occurs.

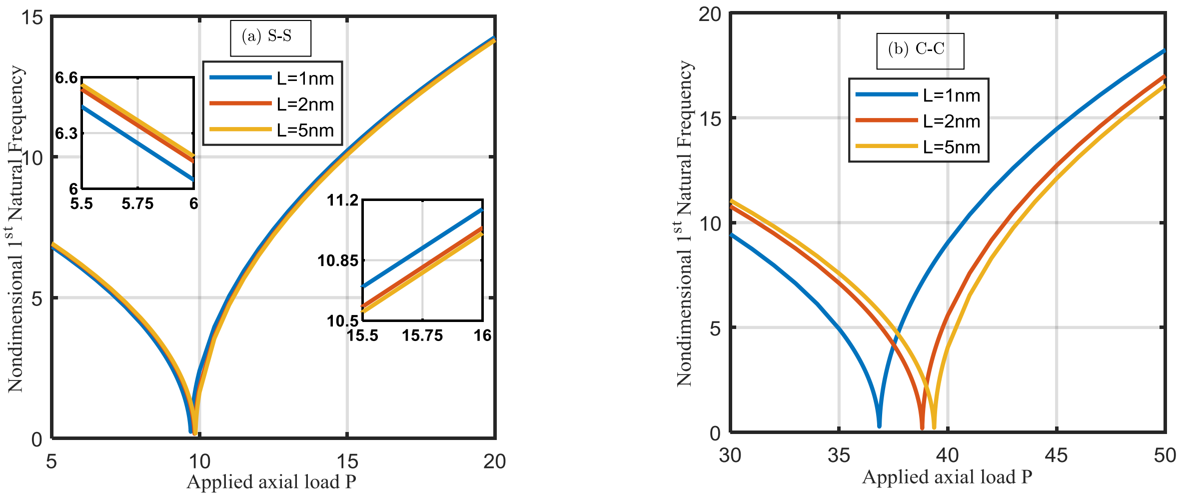

Fig. 6 Influence of length scale on the first natural frequency of S-S and C-C perfect CNT when $k_s = 0$

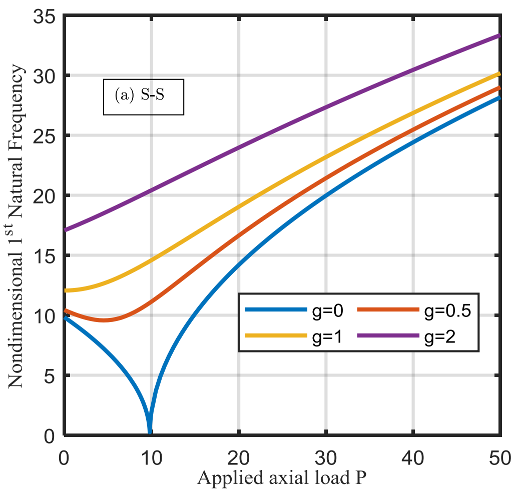

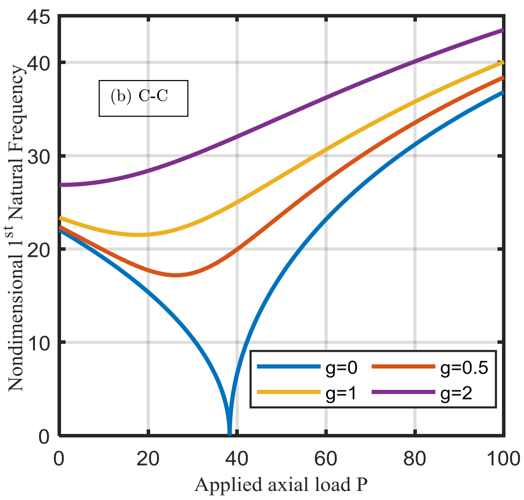

Fig. 7 Influence of imperfection amplitude on the first natural frequency of S-S and C-C imperfect CNT ($k_s = 0, L = 1.5\ nm$)

The influence of imperfection amplitude on the dimensionless first natural frequency of S-S and C-C CNTs is presented in Fig. 7. Fig. 7 shows that increasing the imperfection amplitude results in increasing the first natural frequency of imperfect CNTs.

5. Conclusions

The buckling, post-buckling response and linear vibration behavior of perfect and imperfect CNTs were examined numerically based on DM theory. Different set of boundery conditions were taken into account. The DIQM in conjcution with Newton method is employed to solve nonlinear six-order integro-differential equation governing the buckling problem, and derive the critical buckling load and post-buckling configurations. The DIQM is exploited to discrtize the linear vibration problem and the natural frequencies and corresponding mode shapes were obtained. Some verification studies were conducted for the present method. The results indicates that the DIQM is an efficient techniquce for analyzing the static and dynamic behaviors of CNTs.

The influences of length scale parameter, imperfection amplitude and shear foundation constant on static and dynamic behaviors of CNTs were studied and the following remarks have been obtained

(a) The trend of buckling load of perfect and imperfect CNTs with respect to shear foundation constant is ascending and it is descending with respect to length scale parameter β.
(b) The buckling load has firstly ascending trend followed by descending trend with respect to the amplitude of initial imperfection g.
(c) The absolute values of the amplitude of stable responses of perfect and imperfect CNTs has ascending trend with increasing the length scale parameter (i.e., decreasing the CNTs length).
(d) As the shear foundation constant increases, the natural frequencies increase particularly at higher modes.
(e) The natural frequency has a descending trend with increasing the length scale parameter in the pre-buckling state. The reverse scenario occurs in the post-buckling state.
(f) The natural frequency around the upper branch of imperfect CNTs increases as the imperfection amplitude increases.
(g) The length scale parameter has the most effect on the static and dynamic behaviors of CNTs with C - C boundary conditions.

Acknowledgments

This work was supported by the Deanship of Scientific Research (DSR), King Abdulaziz University, Jeddah, under Grant no. (G-051-135-1441). The authors, therefore, gratefully acknowledge the DSR technical and financial support.

References

Agwa, M.A. and Eltaher, M.A. (2016), “Vibration of a carbyne nanomechanical mass sensor with surface effect”, *Appl. Phys. A*, **122**(4), 335. https://doi.org/10.1007/s00339-016-9934-9

Akgöz, B. and Civalek, Ö. (2011), “Application of strain gradient elasticity theory for buckling analysis of protein microtubules”, *Current Appl. Phys.*, **11**(5), 1133-1138. https://doi.org/10.1016/j.cap.2011.02.006

Akgöz, B. and Civalek, Ö. (2018), “Vibrational characteristics of embedded microbeams lying on a two-parameter elastic foundation in thermal environment”, *Compos. Part B: Eng.*, **150**, 68-77. https://doi.org/10.1016/j.compositesb.2018.05.049

Ameri, A., Ajori, S. and Ansari, R. (2020), “On the buckling behavior of functionalized single-and double-walled carbon nanotubes with azobenzene in the aqueous environment: a molecular dynamics study”, *Struct. Chem.*, **31**(1), 371-384. https://doi.org/10.1007/s11224-019-01418-6

Amir, S., Arshid, E. and Arani, M.R.G. (2019), “Size-dependent magneto-electro-elastic vibration analysis of FG saturated porous annular/circular micro sandwich plates embedded with nano-composite face sheets subjected to multi-physical pre loads”, *Smart Struct. Syst., Int. J.*, **23**(5), 429-447.

https://doi.org/10.12989/sss.2019.23.5.429

Arani, A.G., Pourjamshidian, M., Arefi, M. and Arani, M.R. (2019), "Application of nonlocal elasticity theory on the wave propagation of flexoelectric functionally graded (FG) timoshenko nano-beams considering surface effects and residual surface stress", *Smart Struct. Syst., Int. J.*, **23**(2), 141-153. https://doi.org/10.12989/sss.2019.23.2.141

Arda, M. and Aydogdu, M. (2020), "Vibration analysis of carbon nanotube mass sensors considering both inertia and stiffness of the detected mass", *Mech. Based Des. Struct. Mach.*, 1-17. https://doi.org/10.1080/15397734.2020.1728548

Atkins, P.W. and Friedman, R.S. (2011), *Molecular Quantum Mechanics*, Oxford University Press.

Aydogdu, M. and Gul, U. (2018), "Buckling analysis of double nanofibers embeded in an elastic medium using doublet mechanics theory", *Compos. Struct.*, **202**, 355-363. https://doi.org/10.1016/j.compstruct.2018.02.015

Aydogdu, M. and Gul, U. (2020), "Longitudinal vibration of double nanorod systems using doublet mechanics theory", *Struct. Eng. Mech., Int. J.*, **73**(1), 37-52. https://doi.org/10.12989/sem.2020.73.1.037

Boussoula, A., Boucham, B., Bourada, M., Bourada, F., Tounsi, A., Bousahla, A.A. and Tounsi, A. (2020), "A simple nth-order shear deformation theory for thermomechanical bending analysis of different configurations of FG sandwich plates", *Smart Struct. Syst., Int. J.*, **25**(2), 197-218. https://doi.org/10.12989/sss.2020.25.2.197

Civalek, Ö., Uzun, B., Yaylı, M.Ö. and Akgöz, B. (2020), "Size-dependent transverse and longitudinal vibrations of embedded carbon and silica carbide nanotubes by nonlocal finite element method", *Eur. Phys. J. Plus*, **135**(4), 381. https://doi.org/10.1140/epjp/s13360-020-00385-w

Eberhardt, O. and Wallmersperger, T. (2014), "Mechanical properties and deformation behavior of carbon nanotubes calculated by a molecular mechanics approach", *Smart Struct. Syst., Int. J.*, **13**(4), 685-709. https://doi.org/10.12989/sss.2014.13.4.685

Ellali, M., Amara, K., Bouazza, M. and Bourada, F. (2018), "The buckling of piezoelectric plates on pasternak elastic foundation using higher-order shear deformation plate theories", *Smart Struct. Syst., Int. J.*, **21**(1), 113-122. https://doi.org/10.12989/sss.2018.21.1.113

Eltaher, M.A. and Agwa, M.A. (2016), "Analysis of size-dependent mechanical properties of CNTs mass sensor using energy equivalent model", *Sensors Actuat. A: Phys.*, **246**, 9-17. https://doi.org/10.1016/j.sna.2016.05.009

Eltaher, M.A. and Mohamed, N (2020a), "Vibration of nonlocal perforated nanobeams with general boundary conditions", *Smart Struct. Syst., Int. J.*, **25**(4), 501-514. https://doi.org/10.12989/sss.2020.25.4.501

Eltaher, M.A. and Mohamed, N. (2020b), "Nonlinear stability and vibration of imperfect CNTs by Doublet mechanics", *Appl. Mathe. Computat.*, **382**, 125311. https://doi.org/10.1016/j.amc.2020.125311

Eltaher, M.A., Mahmoud, F.F., Assie, A.E. and Meletis, E.I. (2013), "Coupling effects of nonlocal and surface energy on vibration analysis of nanobeams", *Appl. Mathe. Computat.*, **224**, 760-774. https://doi.org/10.1016/j.amc.2013.09.002

Eltaher, M.A., Khairy, A., Sadoun, A.M. and Omar, F.A. (2014a), "Static and buckling analysis of functionally graded Timoshenko nanobeams", *Appl. Mathe. Computat.*, **229**, 283-295. http://dx.doi.org/10.1016/j.amc.2013.12.072

Eltaher, M.A., Hamed, M.A., Sadoun, A.M. and Mansour, A. (2014b), "Mechanical analysis of higher order gradient nanobeams", *Appl. Mathe. Computat.*, **229**, 260-272. http://dx.doi.org/10.1016/j.amc.2013.12.076

Eltaher, M.A., El-Borgi, S. and Reddy, J.N. (2016a), "Nonlinear analysis of size-dependent and material-dependent nonlocal CNTs", *Compos. Struct.*, **153**, 902-913. http://dx.doi.org/10.1016/j.compstruct.2016.07.013

Eltaher, M.A., Agwa, M.A. and Mahmoud, F.F. (2016b), "Nanobeam sensor for measuring a zeptogram mass", *Int. J. Mech. Mater. Des.*, **12**(2), 211-221. https://doi.org/10.1007/s10999-015-9302-5

Eltaher, M.A., Agwa, M. and Kabeel, A. (2018), "Vibration analysis of material size-dependent CNTs using energy equivalent model", *J. Appl. Computat. Mech.*, **4**(2), 75-86. https://doi.org/10.22055/JACM.2017.22579.1136

Eltaher, M.A., Almalki, T.A., Ahmed, K.I. and Almitani, K.H. (2019a), "Characterization and behaviors of single walled carbon nanotube by equivalent-continuum mechanics approach", *Adv.in Nano Res., Int. J.*, **7**(1), 39-49. https://doi.org/10.12989/anr.2019.7.1.039

Eltaher, M.A., Almalki, T.A., Almitani, K.H., Ahmed, K.I.E. and Abdraboh, A.M. (2019b), "Modal participation of fixed–fixed single-walled carbon nanotube with vacancies", *Int. J. Adv. Struct. Eng.*, **11**(2), 151-163. https://doi.org/10.1007/s40091-019-0222-8

Eltaher, M.A., Almalki, T.A., Almitani, K.H. and Ahmed, K.I.E. (2019c), "Participation factor and vibration of carbon nanotube with vacancies", *J. Nano Res.*, **57**, 158-174. https://doi.org/10.4028/www.scientific.net/JNanoR.57.158

Eltaher, M.A., Mohamed, N., Mohamed, S. and Seddek, L.F. (2019d), "Postbuckling of curved carbon nanotubes using energy equivalent model", *J. Nano Res.*, **57**, 136-157. https://doi.org/10.12989/sem.2019.70.6.737

Eltaher, M.A., Mohamed, N., Mohamed, S.A. and Seddek, L.F. (2019e), "Periodic and nonperiodic modes of postbuckling and nonlinear vibration of beams attached to nonlinear foundations", *Appl. Mathe. Model.*, **75**, 414-445. https://doi.org/10.1016/j.apm.2019.05.026

Eltaher, M.A., Omar, F.A., Abdraboh, A.M., Abdalla, W.S. and Alshorbagy, A.E. (2020), "Mechanical behaviors of piezoelectric nonlocal nanobeam with cutouts", *Smart Struct. Syst., Int. J.*, **25**(2), 219-228. https://doi.org/10.12989/sss.2020.25.2.219

Emam, S.A., Eltaher, M.A., Khater, M.E. and Abdalla, W.S. (2018), "Postbuckling and free vibration of multilayer imperfect nanobeams under a pre-stress load", *Appl. Sci.*, **8**(11), 2238. https://doi.org/10.3390/app8112238

Eringen, A.C. (1972), "Nonlocal polar elastic continua", *Int. J. Eng. Sci.*, **10**(1), 1-16. https://doi.org/10.1016/0020-7225(72)90070-5

Fatahi-Vajari, A. and Imam, A. (2016a), "Axial vibration of single-walled carbon nanotubes using doublet mechanics", *Indian J. Phys.*, **90**(4), 447-455. https://doi.org/10.1007/s12648-015-0775-8

Fatahi-Vajari, A. and Imam, A. (2016b), "Torsional vibration of single-walled carbon nanotubes using doublet mechanics", *Zeitschrift für angewandte Mathematik und Physik*, **67**(4), 81. https://doi.org/10.1007/s00033-016-0675-6

Ferrari, M., Granik, V.T., Granik, V.T., Imam, A. and Nadeau, J.C. (Eds.) (1997), *Advances in Doublet Mechanics*, (Vol. 45), Springer Science & Business Media.

Gao, G., Cagin, T. and Goddard III, W.A. (1998), "Energetics, structure, mechanical and vibrational properties of single-walled carbon nanotubes", *Nanotechnology*, **9**(3), 184. https://doi.org/10.1088/0957-4484/9/3/007

Granik, V.T. and Ferrari, M. (1993), "Microstructural mechanics of granular media", *Mech. Mater.*, **15**(4), 301-322. https://doi.org/10.1016/0167-6636(93)90005-C

Gul, U. and Aydogdu, M. (2017), "Wave propagation in double walled carbon nanotubes by using doublet mechanics theory", *Physica E: Low-dimens. Syst. Nanostruct.*, **93**, 345-357. https://doi.org/10.1016/j.physe.2017.07.003

Gul, U. and Aydogdu, M. (2018a), "Structural modelling of

nanorods and nanobeams using doublet mechanics theory", *Int. J. Mech. Mater. Des.*, **14**(2), 195-212. https://doi.org/10.1007/s10999-017-9371-8
Gul, U. and Aydogdu, M. (2018b), "Noncoaxial vibration and buckling analysis of embedded double-walled carbon nanotubes by using doublet mechanics", *Compos. Part B: Eng.*, **137**, 60-67. https://doi.org/10.1016/j.compositesb.2017.11.005
Gul, U. and Aydogdu, M. (2019), "Vibration analysis of Love nanorods using doublet mechanics theory", *J. Brazil. Soc. Mech. Sci. Eng.*, **41**(8), 351. https://doi.org/10.1007/s40430-019-1849-x
Gul, U., Aydogdu, M. and Gaygusuzoglu, G. (2017), "Axial dynamics of a nanorod embedded in an elastic medium using doublet mechanics", *Compos. Struct.*, **160**, 1268-1278. https://doi.org/10.1016/j.compstruct.2016.11.023
Gul, U., Aydogdu, M. and Gaygusuzoglu, G.J.J.o.E.M. (2018), "Vibration and buckling analysis of nanotubes (nanofibers) embedded in an elastic medium using Doublet Mechanics", *J. Eng. Mathe.*, **109**(1), 85-111. https://doi.org/10.1007/s10665-017-9908-8
Gurtin, M.E. and Murdoch, A.I. (1975), "A continuum theory of elastic material surfaces", *Arch. Rational Mech. Anal.*, **57**(4), 291-323. https://doi.org/10.1007/BF00261375
Hehre, W.J. (1976), "Ab initio molecular orbital theory", *Accounts Chem. Res.*, **9**(11), 399-406. https://doi.org/10.1021/ar50107a003
Iijima, S. (1991), "Helical microtubules of graphitic carbon", *Nature*, **354**(6348), 56. https://doi.org/10.1038/354056a0
Kojic, M., Vlastelica, I., Decuzzi, P., Granik, V.T. and Ferrari, M. (2011), "A finite element formulation for the doublet mechanics modeling of microstructural materials", *Comput. Methods Appl. Mech. Eng.*, **200**(13-16), 1446-1454. https://doi.org/10.1016/j.cma.2011.01.001
Kresse, G. and Hafner, J. (1993), "Ab initio molecular dynamics for liquid metals", *Phys. Rev. B*, **47**(1), 558. https://doi.org/10.1103/PhysRevB.47.558
Li, C. and Chou, T.W. (2003), "A structural mechanics approach for the analysis of carbon nanotubes", *Int. J. Solids Struct.*, **40**(10), 2487-2499. https://doi.org/10.1016/S0020-7683(03)00056-8
Li, C. and Chou, T.W. (2004), "Modeling of elastic buckling of carbon nanotubes by molecular structural mechanics approach", *Mech. Mater.*, **36**(11), 1047-1055. https://doi.org/10.1016/j.mechmat.2003.08.009
Mehralian, F., Beni, Y.T. and Kiani, Y. (2017), "Molecular dynamics study on the thermal buckling of carbon nanotubes in the presence of pre-load", *Mater. Res. Express*, **4**(1), 015011. https://doi.org/10.1088/2053-1591/aa576a
Mindlin, R.D. (1963), "Influence of couple-stresses on stress concentrations", *Experim. Mech.*, **3**(1), 1-7.
Mohamed, N., Eltaher, M.A., Mohamed, S.A. and Seddek, L.F. (2018), "Numerical analysis of nonlinear free and forced vibrations of buckled curved beams resting on nonlinear elastic foundations", *Int. J. Non-Linear Mech.*, **101**, 157-173. https://doi.org/10.1016/j.ijnonlinmec.2018.02.014
Mohamed, N., Eltaher, M.A., Mohamed, S.A. and Seddek, L.F. (2019), "Energy equivalent model in analysis of postbuckling of imperfect carbon nanotubes resting on nonlinear elastic foundation", *Struct. Eng. Mech.*, *Int. J.*, **70**(6), 737-750. https://doi.org/10.12989/sem.2019.70.6.737
Mohamed, N., Mohamed, S.A. and Eltaher, M.A. (2020), "Buckling and post-buckling behaviors of higher order carbon nanotubes using energy-equivalent model", *Eng. Comput.* https://doi.org/10.1007/s00366-020-00976-2
Peng, S. and Cho, K. (2003), "Ab initio study of doped carbon nanotube sensors", *Nano Lett.*, **3**(4), 513-517. https://doi.org/10.1021/nl034064u
Rapaport, D.C. and Rapaport, D.C.R. (2004), *The Art of Molecular Dynamics Simulation*, Cambridge University Press.
Shokravi, M. (2018), "Dynamic buckling of smart sandwich beam subjected to electric field based on hyperbolic piezoelasticity theory", *Smart Struct. Syst.*, *Int. J.*, **22**(3), 327-334. https://doi.org/10.12989/sss.2018.22.3.327
Shokravi, M. and Jalili, N. (2017), "Dynamic buckling response of temperature-dependent functionally graded-carbon nanotubes-reinforced sandwich microplates considering structural damping", *Smart Struct. Syst.*, *Int. J.*, **20**(5), 583-593. https://doi.org/10.12989/sss.2017.20.5.583
Tabbakh, M. and Nasihatgozar, M. (2018), "Buckling analysis of nanocomposite plates coated by magnetostrictive layer", *Smart Struct. Syst.*, *Int. J.*, **22**(6), 743-751. https://doi.org/10.12989/sss.2018.22.6.743
Tounsi, A., Benguediab, S., Adda, B., Semmah, A. and Zidour, M. (2013), "Nonlocal effects on thermal buckling properties of double-walled carbon nanotubes", *Adv. Nano Res.*, *Int. J.*, **1**(1), 1-11. https://doi.org/10.12989/anr.2013.1.1.001
Toupin, R.A. (1962), "Elastic materials with couple-stresses", *Arch. Rational Mech. Anal.*, **11**(1), 385-414.
Xiao, J.R., Gama, B.A. and Gillespie Jr, J.W. (2005), "An analytical molecular structural mechanics model for the mechanical properties of carbon nanotubes", *Int. J. Solids Struct.*, **42**(11-12), 3075-3092. https://doi.org/10.1016/j.ijsolstr.2004.10.031
Yang, F.A.C.M., Chong, A.C.M., Lam, D.C.C. and Tong, P. (2002), "Couple stress based strain gradient theory for elasticity", *Int. J. Solids Struct.*, **39**(10), 2731-2743. https://doi.org/10.1016/S0020-7683(02)00152-X
Yayli, M.Ö. and Asa, E. (2019), "Longitudinal vibration of carbon nanotubes with elastically restrained ends using doublet mechanics", *Microsyst. Technol.*, 1-10. https://doi.org/10.1007/s00542-019-04512-1
Youcef, D.O., Kaci, A., Benzair, A., Bousahla, A.A. and Tounsi, A. (2018), "Dynamic analysis of nanoscale beams including surface stress effects", *Smart Struct. Syst.*, *Int. J.*, **21**(1), 65-74. https://doi.org/10.12989/sss.2018.21.1.065
Zhou, L.G. and Shi, S.Q. (2002), "Molecular dynamic simulations on tensile mechanical properties of single-walled carbon nanotubes with and without hydrogen storage", *Computat. Mater. Sci.*, **23**(1-4), 166-174. https://doi.org/10.1016/S0927-0256(01)00233-6

CC

Appendix A

Analytical solutions for C-S perfect CNT

Following Eltaher and Mohamed (2020b), the analytical solution for buckling problem of C-S perfect CNTs can be obtained. By removing the geometric imperfection w_0 from buckling problem (19), that is

$$\beta^2 w_s^{vi} + w_s^{iv} + \lambda^2 w_s'' = 0 \tag{A1}$$

$$\lambda^2 = P - k_s - \frac{1}{2}\int_0^1 w_s'^2 dx \tag{A2}$$

The solution of Eq. (A1) can be written as

$$w_s(x) = c_1 + c_2 x + c_3 sin(s_1 x) + c_4 cos(s_1 x) + c_5 sin(s_2 x) + c_6 cos(s_2 x) \tag{A3}$$

in which

$$s_{1,2} = \frac{1}{\beta}\sqrt{\frac{1}{2}\left(1 \pm \sqrt{1 - 4\beta^2\lambda^2}\right)} \tag{A4}$$

To compute the constants $c_i, (i = 1,2, \dots 6)$, applying the C-S boundary conditions Eq. (22), yields the following nonlinear eigenvalue problem

$$\begin{bmatrix} 1 & 0 & 0 & 1 & 0 & 1 \\ 0 & 1 & s_1 & 0 & s_2 & 0 \\ 0 & 0 & s_1^3 & 0 & s_2^3 & 0 \\ 1 & 1 & \sin(s_1) & \cos(s_1) & sin(s_2) & \cos(s_2) \\ 0 & 0 & s_1^2 sin(s_1) & s_1^2 cos(s_1) & s_2^2 sin(s_2) & s_2^2 cos(s_2) \\ 0 & 0 & s_1^2 \delta_1 sin(s_1) & s_1^2 \delta_1 cos(s_1) & s_2^2 \delta_2 sin(s_2) & s_2^2 \delta_2 cos(s_2) \end{bmatrix} \begin{bmatrix} c_1 \\ c_2 \\ c_3 \\ c_4 \\ c_5 \\ c_6 \end{bmatrix} = \begin{bmatrix} 0 \\ 0 \\ 0 \\ 0 \\ 0 \\ 0 \end{bmatrix} \tag{A5}$$

where

$$\delta_1 = (1 - \beta^2 s_1^2) \text{ and } \delta_2 = (1 - \beta^2 s_2^2)$$

The determinant of Eq. (A5) is set to zero, yields the following characteristic equation

$$s_1^3(tan(s_2) - s_2) - s_2^3(tan(s_1) - s_1) = 0 \tag{A6}$$

Solving Eq. (A6) numerically, the values of λ can be computed. And hence the critical buckling load of C-S perfect CNTs is calculated as

$$P_c = k_s + \lambda^2 \tag{A7}$$

The mode shapes can be obtained as

$$\begin{aligned} w_s(x) = c\Bigg(1 - x - \frac{(1 - \beta^2 s_1^2)}{(1 - 2\beta^2 s_1^2)s_1} sin(s_1 x) - \frac{(1 - \beta^2 s_1^2)}{(1 - 2\beta^2 s_1^2)s_1} tan(s_1) cos(s_1 x) \\ - \frac{\beta^2 s_1^2}{(1 - 2\beta^2 s_1^2)s_2} sin(s_2 x) + \frac{\beta^2 s_1^2}{(1 - 2\beta^2 s_1^2)s_2} tan(s_2) cos(s_2 x)\Bigg) \end{aligned} \tag{A8}$$

where the first mode shape of C-S perfect CNT is obtained by substituting the smallest value of λ computed from Eq. (A6) into Eq. (A8). The initial imperfection w_0 of C-S CNT is taken to be the first mode shape obtained from Eq. (A8).